Enhanced Cooling of Electronic Chips Using Combined Diamond Coating and Microfluidics

Dor Daniel,[1] Albert Mosyak,[1] Roza Akhvlediani,[2] Alon Hoffman,[2] and Gilad Yossifon[1,*]

[1] *Faculty of Mechanical Engineering, Technion, Israel Institute of Technology, Haifa 32000, Israel*
[2] *Schulich Faculty of Chemistry, Technion-Israel Institute of Technology, Haifa 32000, Israel*

(Received 17 June 2018; revised manuscript received 14 December 2018; published 24 January 2019)

We investigate the impact of the combined diamond heat-spreading layer and microfluidic convection on the performance of a model electronic chip heated locally. Experiments are carried out and a finite element method is used to simulate the thermal response of the device under transient step-wise (without flow) and steady-state (with flow) operation conditions up to heat flux values of 38 and 190 W/cm^2, respectively. In all cases, the temperature on the heated outer silicon surface did not exceed 100 °C. The temperature field contour has an oval shape for transient heating without flow and a funnel shape for steady-state heating with flow. For a step-wise heat flux of 38 W/cm^2, the differences between temperatures at the center of the resistor and at the outer surface edge after a time interval of 8 s are 5, 3, and 1 °C for the chips without a diamond layer, with a 100-μm diamond layer, and only a 400-μm diamond, respectively, which proves the enhanced spreading due to the diamond layer. Under steady-state conditions at a heat flux of 190 W/cm^2 and volumetric flow rates of water between 2 and 5 ml/min, the surface temperature decreases by approximately15% for silicon wafer with a 100-μm diamond layer and by approximately 22% for a 400-μm diamond as compared to heating without the addition of diamond. Of crucial importance is the proximity of the diamond layer to the heat source, which makes this method advantageous over other thermal management procedures, especially for pulsed operating conditions and hot spots.

DOI: 10.1103/PhysRevApplied.11.014047

I. INTRODUCTION

The increased integration density of electronic components and subsystems has exacerbated the thermal management challenges facing electronic system developers. The confluence of chip power dissipation above 100 W and localized hot spots exposes the limitations of current cooling methods [1]. To overcome these limitations, it is essential to cool the on-chip heat generation sites and dissipate the extracted heat. Microchannel heat sinks are excellent candidates for dissipation of the high heat fluxes anticipated in high-power electronic devices [2].

Development of advanced systems such as directed energy weapons (DEW) and radar using wide band-gap semiconductors (WBS) highlights the necessity for innovation in thermal management in the high flux regime (up to 1 kW/cm^2) and into the ultra-high (up to 100 kW/cm^2) regime [3]. Recent development activities require heat removal from diode arrays and electromagnetic weapons of 1700 W/cm^2 over small areas typical of thermal diodes, and 500 W/cm^2 over large areas in tube collector regions [4]. To dissipate the concentrated high heat flux, the effective heat spreading capability is quite significant. A diamond heat spreader of high thermal conductivity turns out to be a great candidate for this application.

Radar and communication transistor applications are often dominated by pulsed-device operation, with pulse lengths on the order of 10–250 μs for radar and submicroseconds to milliseconds for communication applications. Time-dependent information is of particular relevance for Gallium Nitride (GaN) systems, Blackburn [5], Kuball *et al.* [6]. Although transients might be very rapid during heat transfer within microchannels due to the short length scale involved, conjugation effects might play a major role in the transient behavior of thermal microsystems, considerably increasing the duration of the thermal responses to different time-wise disturbances [7]. This further motivates the use of diamond layers that can rapidly spread the transient heat generation. Here, we focus on combining both a microchannel heat sink and a diamond heat spreader for enhanced cooling under both transient and steady-state conditions.

In particular, GaN-based field-effect transistors have demonstrated extremely high-power densities at microwave frequencies with self-heating being one of the limitations during operation. Several attempts have been reported on the thermal management of GaN heterostructures using diamond films mostly based on technologies such as

*yossifon@tx.technion.ac.il

 © 2019 American Physical Society

atomically bonding GaN epitaxial layers to polycrystalline diamond [8] obtained using chemical vapor deposition (CVD) or by direct growth by molecular beam epitaxy (MBE) on a single-crystal diamond [9]. The steady-state thermal resistance of a small heat source applied to a diamond heat spreader attached to a larger substrate with natural convection cooling on the opposite side was evaluated using numerical simulation by Rogacs and Rhee [10].

Another alternative would be the direct growth of diamond on top of the GaN HEMT (high electron mobility transistor) structure, thus locating the heat sink in close proximity to the channel and avoiding thermal barriers such as the GaN buffer layer or the wafer bonding-interface material. Wang *et al*. numerically investigated the impact of diamond heat-spreading layers on the performance of (Al, Ga)N/GaN high-electron-mobility transistors [11] and showed a maximum temperature reduction of approximately 30% at the drain edge of the gate for a device with a 5-μm diamond layer. Although several studies demonstrated successful growth of diamond layers at either approximately 500 °C [12] or at a higher temperature range of 750 to 800 °C [13] and their compatibility with state-of-the-art GaN device-processing technology with no observable degradation or changes in the HEMT dc characteristics [13], the harsh environmental conditions of high temperature pose a limitation on the growth rate and maximum thickness of the diamond layer and is, in general, not compatible with other non-GaN-based structures. Hence, herein we focus on the former alternative of using the diamond films as heat spreaders below the substrate of the active layer.

Very few experimental works exist on the use of microchannel cooling for dealing with the localized heat fluxes. Goodson *et al*. [14] performed calculations for the system of microchannels within the diamond rather than within silicon. The thermal analysis predicted that the proposed diamond microchannel cooling systems yield remarkable heat-sinking improvement for the high-power laser diode arrays compared to the cooling system fabricated using the silicon technique. Experiments on removing high heat fluxes from GaN-on-silicon carbide (SIC) semiconductor dies using microchannels were described by Calame *et al*. [15]. The diamond was attached to the microchannel cooler using Sn-3.5Ag solder (thermal conductivity of 33 W/m K) with a thickness of 50 μm. It was shown that adding the diamond layer on top of a silicon microchannel greatly improved the heat transfer characteristics compared to silicon by itself. A diamond heat spreader was applied by Y. Han *et al*. [16] on the Si-hybrid microcooler for the improvement of the hotspots' cooling capability for GaN devices. However, to the best of our knowledge, a comprehensive study of transient and steady-state conditions, localized heating, and combined microchannel cooling and diamond heat spreader of varying diamond thicknesses has not been reported.

We use the finite element method implemented in commercial simulation software (COMSOL) to investigate the potential reduction of hot spots' temperature using a diamond layer and microchannel heat sink. In Sec. II, the simulation details are described. Chip fabrication and experimental methodology are presented in Sec. III. Experimental results compared to COMSOL simulation are shown and discussed in Sec. IV. Conclusions on the improvement of heat-dissipation capability using the diamond heat spreader on a Si-hybrid microcooler are given in Sec. V.

II. NUMERICAL SIMULATIONS

The simulation models are constructed using the finite-element-based commercial software COMSOL. The built-in fluid flow and heat transfer interfaces are used in a three-dimensional (3D) model that couples both solid and fluid parts (see Fig. S1 in the Supplemental Material [17]). These are summarized for both the case of no flow, which was used for studying the system transient response, and the steady-state case with flow. The solution is tested for mesh independence by reducing the mesh size by one half. The velocities and the temperatures match within 99.6% for both the mesh sizes. The models use 3D geometry where creeping flow along with the incompressibility condition are used with the following governing equations:

$$-\nabla p + \mu \Delta \mathbf{u} = 0, \tag{1}$$

$$\nabla \mathbf{u} = 0, \tag{2}$$

$$\partial T/\partial t + \mathbf{u} \cdot \Delta T = \alpha \Delta T, \tag{3}$$

where p is the pressure, μ is the dynamic viscosity, $\mathbf{u}$ is the velocity vector, T is the temperature, t is the time, and α is the thermal diffusivity. For the solid domains [polydimethylsiloxane (PDMS), Si and diamond], the governing equation is the heat equation, Eq. (3) with $\mathbf{u} = 0$, and the corresponding thermal conductivity (Table I). It should be noted that there is variability in the value of diamond thermal conductivity used in different studies. For example, Han *et al*. [16] analyzed four types of diamond heat spreaders. The first three types were in the range of 1500–2000 W/m K and the fourth was 1000 W/m K, all at room temperature. The cooling capabilities of the structure with types 1–3 were quite similar. With the type-4 diamond heat spreader at a power of 110 W, the maximum hot spot temperature is higher by 3.2% than that of type 1. Here, we used a nominal diamond thermal conductivity of 1500 W/m K [19].

The boundary conditions are constant heat flux generation on the heater surface ($q'' = P/A_{\text{resistor}}$) and natural convection with radiation from the external surfaces

$$q'' = h(T_s - T_\infty) + \sigma \cdot \varepsilon \cdot (T_s^4 - {T_\infty}^4), \tag{4}$$

where T_s is the surface temperature, T_∞ is the ambient tem-

TABLE I. Thermal properties of components (at $T = 23$ °C) [18].

Item	Silicon	PDMS	Diamond	Water	Air
k(W/mK)	149	0.15	1500	0.6	0.026
c_p (J/kg K)	700	1460	500	4200	1000
ρ (kg/m^3)	2329	965	3515	997	1.2

perature, σ is the Stefan-Boltzmann constant, and $\varepsilon = 0.95$ is the emissivity of external surfaces. For the upper surface ($z = 0$), we use the calculated value $h = 20$ W/m^{2}K, and use $h = 10$ W/m^2 K on other surfaces [18]. The mass flow is taken as constant, the temperature at the inlet $T = 23$ °C, and the thermal condition at the outlet $dT/dz = 0$.

III. EXPERIMENTAL METHODOLOGY

A. Diamond film deposition

Diamond film deposition is performed using the home-made hot-filament chemical-vapor deposition (HF CVD) system previously described [20] using a methane-hydrogen gas mixture at a 1:99 vol.% onto silicon substrates. The substrate temperature during deposition is approximately 750 °C and the growth rate is approximately 1 μm/h. Prior to deposition, the silicon substrate surfaces are seeded by ultrasonification with a mixed diamond slurry [21], which results in an initial diamond particle density formation of approximately 10^{10} cm^{-2}. With increasing deposition time and the competition of growth nuclei, the aerial particle density decreases to approximately 10^8 cm^{-2}. The 400-μm-thick freestanding films are obtained by etching the silicon substrate following

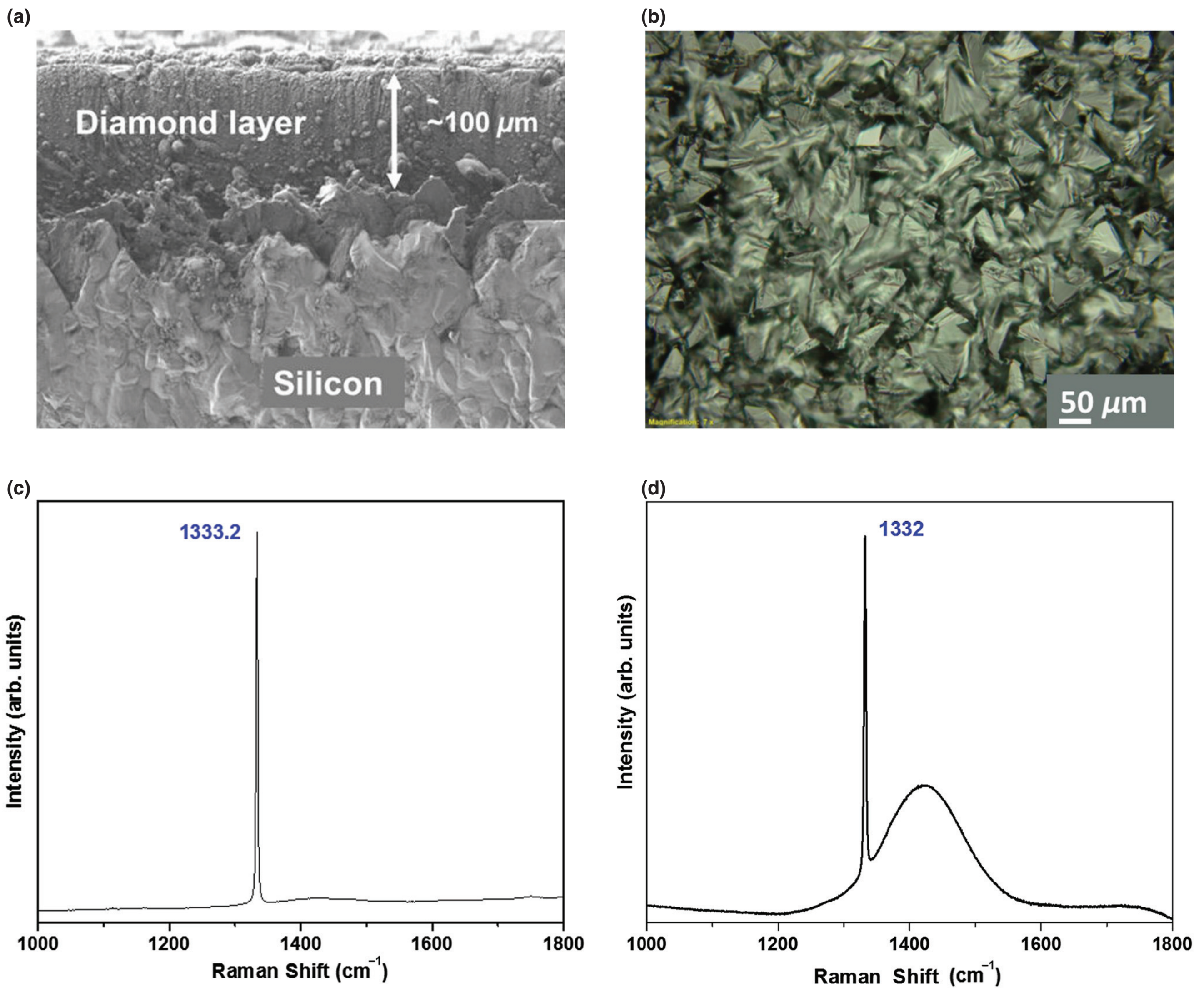

FIG. 1. Silicon with polycrystalline a diamond film layer 100-μm thick. (a) Cross-section HR SEM image and (b) top view. Micro-Raman spectra of polycrystalline diamond film (c) of 100-μm and (d) 400-µm-thick deposited onto a silicon substrate.

TABLE II. Dimensions (in mm) of the device structure shown in Fig. 2.

System	A	B	C	D	E	H	W
Silicon	0	0.4	3	16	10	0.35	6
Silicon with layer of 100-μm diamond	0.1	0.4	3	16	10	0.35	6
With only 400-μm diamond	0.4	0	3	16	10	0.35	6

deposition. A cross-section high-resolution scanning electron micrograph (HR SEM) of the 100-μm-thick film is shown in Fig. 1(a). From this figure, the columnar structure of the films can be clearly seen. A top-view HR SEM of the 100-μm-thick film is shown in Fig 1(b). As can be seen, the diamond grain areal size at the film surface is a few 10s of μm^2. The roughness of the as-deposited film is 1–2 μm using Surface Profiler (KLA Tencor Alpha-Step 500).

In Fig. 1(c), the Raman spectrum (incident photon wavelength of 532 nm) of the film is shown. The spectrum is dominated by a sharp peak at 1333.2 cm^{-1}, which is characteristic of diamond, evidencing the very high-quality crystallinity of the deposited film. The Raman spectrum of the 400-μm-thick film and morphology are similar to that of the 100-μm-thick film (not shown).

B. Test device

The experimental tests are carried out on the chip with a diamond spreader located on top of the silicon wafer. The sizes of the chip components are listed in Table II. The microheater is built on the center of the diamond spreader, Fig. 2. An electric resistor, which is used as a heat source made of Au-Cr, is attached to the diamond surface by standard photolithography technique and is connected to an electric source. The heater has dimensions of 200 nm in thickness, 0.7 mm in width, and a length of 7 mm. The space between each part of the resistor is 0.1 mm [Fig. 3(a)] and its overall heated surface is 4.2 mm^2. The heat sink of the microchannel is 350 μm in height, 6 mm in width, and 7 mm in length. In order to reach uniform flow conditions, a manifold is used as shown in Fig. 3(b). The fluidic system is made of PDMS consisting of a single-wide microchannel, in order to avoid as much as possible the coverage of the Si backside with the thermally-poor-conductive PDMS material, and is bonded to the silicon or diamond backside surface by an oxygen plasma treatment (HF-8, Axic corp.).

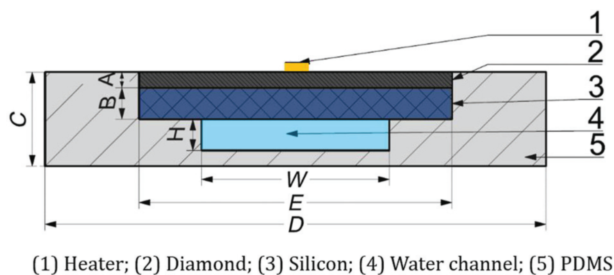

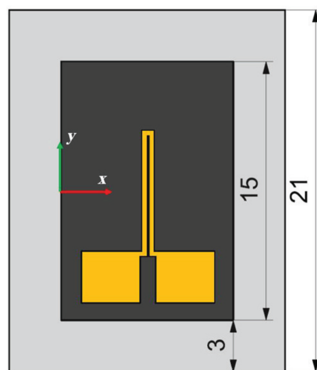

FIG. 2. Schematic of the device: (top) cross section; (bottom) top view. All dimensions are in mm.

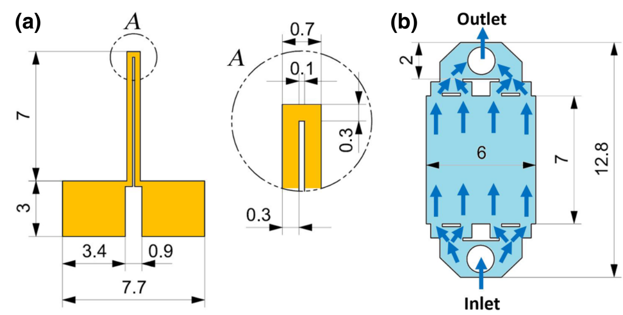

FIG. 3. Details of (a) resistor and (b) manifold geometry.

C. Manifold

Several studies have shown that the manifolds' design plays an important role in the liquid distribution in microchannels, which, if not uniform, can lead to large transverse temperature gradients on the device surface, larger thermal stresses, and reduce the device's reliability [22,23]. In the present study, we use a configuration of the manifolds as illustrated in Fig. 3(b). Such a type of manifolds ensures uniform velocity distribution at the entrance of the microchannels [24,25].

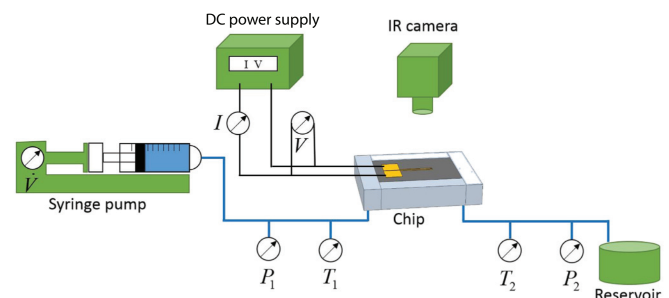

FIG. 4. Experimental setup.

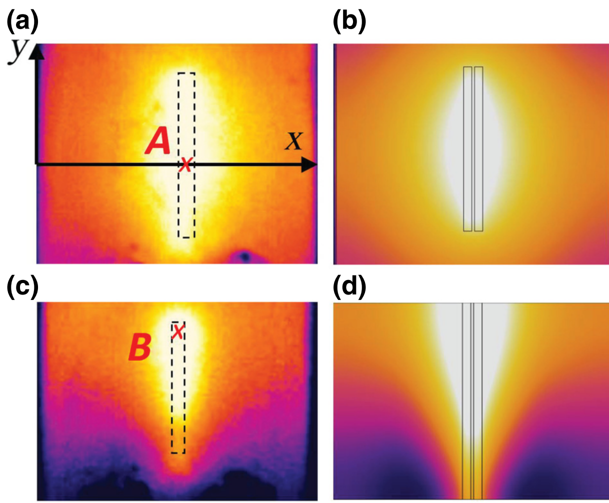

FIG. 5. Qualitative comparison between temperature distributions under transient (a),(b) and steady-state conditions (c),(d).

D. Experimental setup

A schematic of the experimental apparatus is shown in Fig. 4. In steady-state experiments, filtered water at a temperature of $T = 23\,^{\circ}\mathrm{C}$ is used as the working fluid. The water is pumped by a syringe pump through the inlet manifold to the microchannel in the test module, and from the microchannel through the outlet manifold to the exit tank. The volumetric flow rate of the water is set by the syringe pump.

E. Experimental procedure

A thermal imaging radiometer is utilized to complete the study of the temperature field on the outer heated surface with a temperature measurement error which does not exceed 1 K. The camera is suitable for temperature measurements with a frequency of 80 Hz. The measurement resolution is 0.03 mm. The heater and the outer silicon surface are coated with a thin layer of a black diffusive paint with an emissivity of 0.95. The determination of the emissivity is conducted by the method described in detail by Hetsroni *et al.* [26].

For a normal steady-state testing procedure, the pump is turned at volumetric flow rates from 1 to 5 ml/s. The electrical power to the heater is adjusted to a desired level by a variable voltage controller. The test module is then allowed to reach a steady state, which is achieved within about 10 min. The temperatures of the water at the inlet and outlet of the manifolds are measured by thermocouples and the temperature field is recorded by IR radiometer.

In a step-wise application of the power, the microchannel with its inlet and outlet manifolds closed contain air at ambient conditions. The electric power of the heater is adjusted to the desired level. Thereafter, the device is cooled down to the ambient temperature and a step-wise heating is applied. IR thermography is used to directly measure the transient surface temperature, illustrating the influence of the diamond layer on the device thermal dynamics. The total heat balance may be expressed as

$$q_{\text{heater}} = q_{\text{inner flow}} + q_{\text{environment}}, \tag{5}$$

where $q_{\text{heater}} = I \cdot V$ is the Joule heating within the heater (I and V are the input current and voltage, respectively), $q_{\text{inner flow}} = \dot{m} \cdot c_p \cdot (T_{\text{out}} - T_{\text{in}})$ is the heating power transferred to the fluid within the channels (where $\dot{m}$ is the mass flow rate, c_p is the specific heat, T_{out} and T_{in} are the outlet and the inlet temperatures measured by thermocouples), $q_{\text{environment}} = q_{fc} + q_{\text{rad}}$ is the power conducted through the solid body of the test module to the environment due to free convection (q_{fc}) and radiation (q_{rad}). The experimental discrepancy between q_{heater} and $q_{\text{inner flow}} + q_{\text{environment}}$ is between 2.3% and 3.8%, depending on the total energy input from the heater.

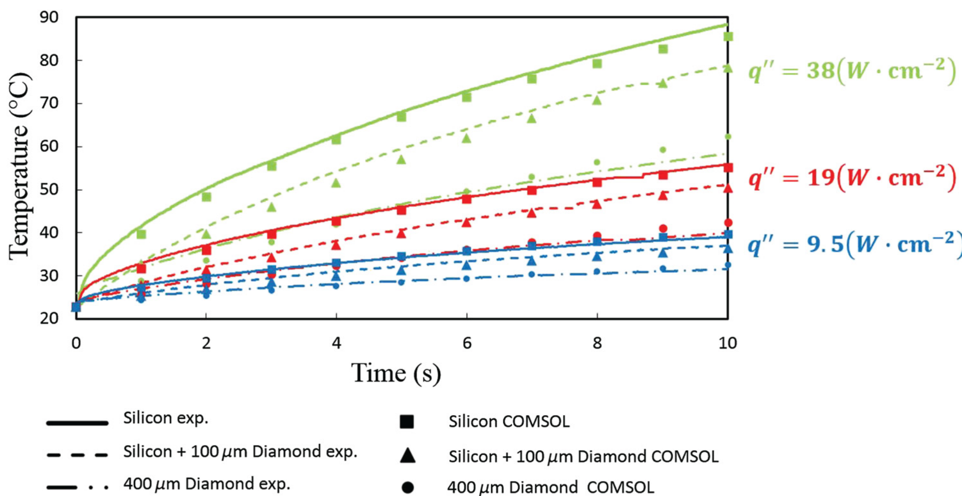

FIG. 6. Transient response of maximum temperature at the heated outer surface for various heater powers and for the three different chip types (Si; Si-diamond; diamond). Experimental results are shown as continuous lines while numerical simulations are depicted as symbols.

IV. RESULTS AND DISCUSSION

A. Qualitative comparison between temperature distribution under transient and steady-state conditions

In the case of transient conditions, there is no forced fluid flow within the microchannel, whereas in the case of steady-state conditions, water is pumped through the microchannel. Figures 5(a) and 5(b) show the temperature field on the heated silicon surface under transient conditions of experimental and simulation results, respectively. Figures. 5(c) and 5(d) show the temperature field under steady-state conditions. The dotted rectangular area in these figures represents the heater. The maximum surface temperature is in the vicinity of points A and B for the transient and steady-state heating, respectively. The contour of the temperature field has an elliptical shape under transient heating and a funnel-like shape for steady-state heating. We see that the numerical simulations agree well with experimental results.

B. Transient response

The transient response of the system is studied by measuring the time variation of the maximum temperature and the temperature spatial distribution along the width of the silicon outer surface for the different chip types at various values of heat flux. The investigation is an attempt to determine if there are significant performance improvements due to the use of diamond layers with immobile air within the microchannels. We present experimental results and numerical simulations on the system transient response to a step-wise application of heat flux during a time interval of 10 s. Figure 6 shows the time dependence of the maximum temperature (see Fig. 5(a) and Fig. S3 in the Supplemental Material [17]) on heat flux. Data at heat fluxes of 38, 19, and 9.5 W/cm^2 are presented by green, red, and blue lines, respectively. The bold lines reflect a case of heating without a diamond layer, the dotted line is a case of heating with a 100-μm diamond layer, and the intermittent line is a case of heating with only a 400-μm diamond layer. Colored symbols represent numerical simulation results. Experimental results agree quite well with numerical simulations. At a time interval of 10 s, the larger effect is at the larger value of heat flux of 38 W/cm^2. The maximum temperature decreases about 15% when using a 100-μm diamond layer and about 34% when using only a 400-μm diamond layer.

Figure 7 shows the temperature distribution on the silicon surface of the device along the x axis [see Figs. 5(c) and 5(d)] at a heat flux of 38 W/cm^2 for different time intervals of heating. Figures 7(a)–7(c) illustrate experimental results (color lines) and numerical simulations (black lines) for cases without a diamond layer, with a 100-μm diamond layer, and with only a 400-μm diamond layer, respectively.

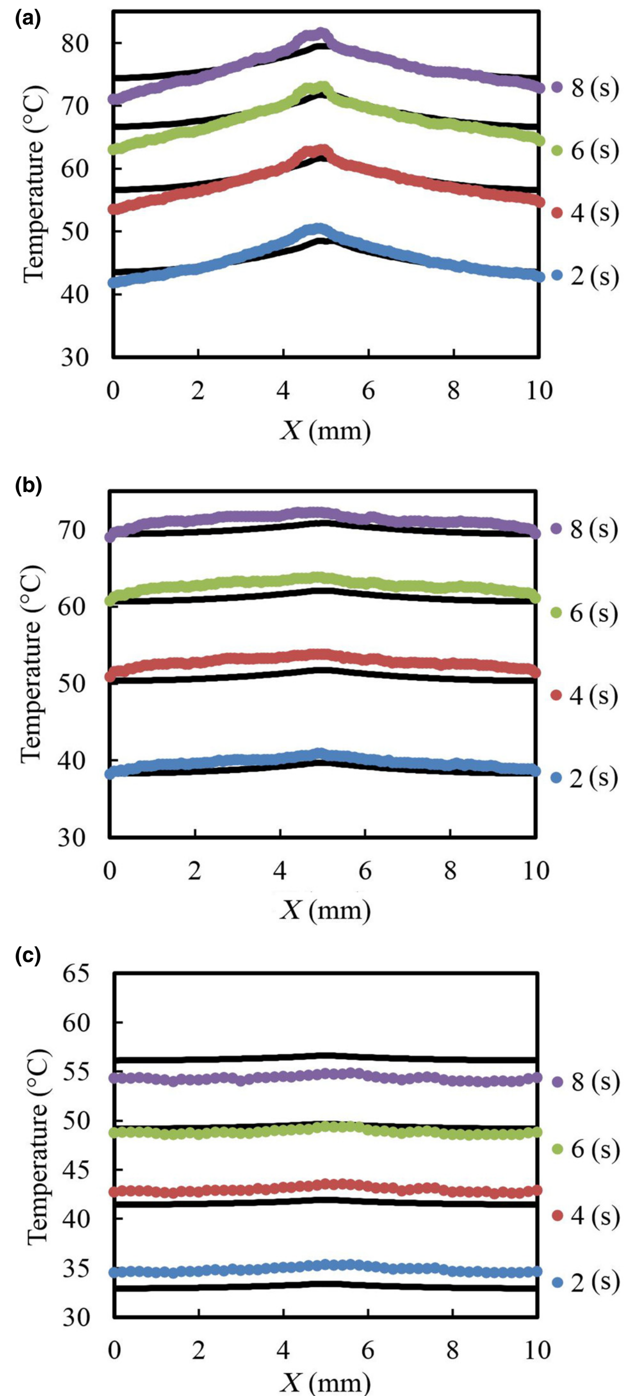

FIG. 7. Temperature spatial distribution on the silicon surface of the device along the x axis at a heat flux of 38 W/cm^2 for different time intervals of heating. Transient response in terms of the measured (color lines) and calculated (black lines) temperature distributions for the three different chip types: (a) Si, (b) Si/diamond, (c) diamond.

There is a good agreement between the experimental and calculation results. The maximum temperature is obtained at the center of the heater. After a time interval of 8 s, the

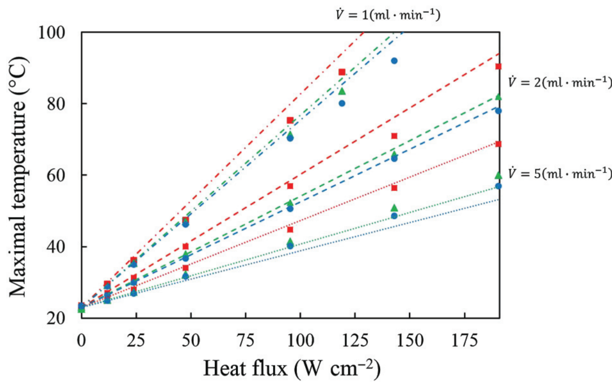

FIG. 8. Steady-state response in terms of the maximum measured temperature vs the heater power for the three different chip types (Si red, Si-diamond green, diamond blue) and various flow rates. Symbols stand for experiments while lines represent numerical simulations.

differences between the temperatures at the center and at the edge of the outer surface are 5, 3, and 1 °C for cases without a diamond layer, with a 100-μm diamond layer, and with only a 400-μm diamond layer, respectively.

C. Steady-state response

Figure 8 shows the dependence of maximum temperature [see Fig. 5(c)] on heat flux at different values of volumetric flow rates. The data for silicon, for silicon with a 100-μm diamond layer, and with only a 400-μm diamond layer are presented as red, green, and blue lines, respectively. The volumetric rates of 5, 2, and 1 ml/min are shown with bold, dotted, and intermittent lines, respectively. Color points represent results of numerical simulations. Experimental results qualitatively agree with numerical simulations. The effect of diamond on the temperature of the heated surface depends on heat flux. At a heat flux of 190 W/cm^2 and flow volume rates of 2–5 ml/min, the surface temperature decreases about 15% for the silicon wafer with a 100-μm diamond layer and about 22% for the 400-μm diamond layer. At a heat flux of 100 W/cm^2 and flow volume rates of 2–5 ml/min, the surface temperature decreases about 11% for a silicon wafer with a 100-μm diamond layer and about 15% for a 400-μm diamond layer as compared to heating without the addition of diamond.

Figure 9 shows the maximum temperature distribution on the silicon surface of the device along the x axis [see Fig. 5(c)] at different powers of the heater and a flow rate of 5 ml/min. Figures 9(a)–9(c) illustrate experimental results (color lines) and numerical simulations (black lines) for cases without a diamond layer, with a 100-μm diamond layer, and with only a 400-μm diamond layer, respectively (see also Fig. S4 in the Supplemental Material [17]). There is good agreement between the experiment and calculations.

V. CONCLUSIONS

The thermal dynamics of a model electronic chip with diamond layers and microfluidic channels is studied. We present experimental results and numerical simulations on the influence of a step-wise application of heater power on the system's transient response. The largest effect measured is at a maximal heat flux of 38 W/cm^2. The maximum temperature decreases about 15% using a 100-μm

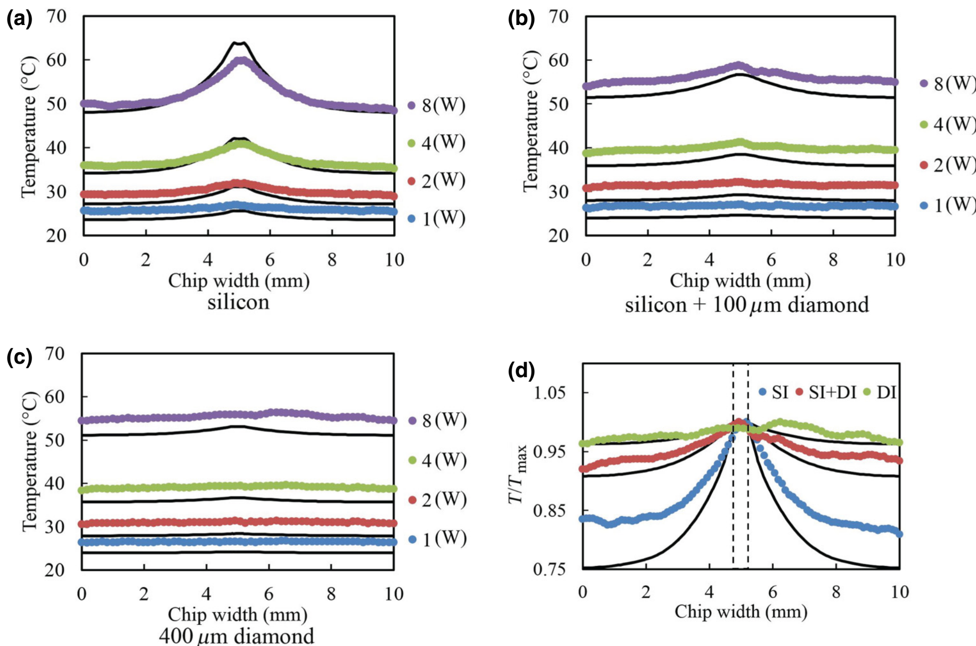

FIG. 9. Steady-state response in terms of the temperature distributions for the three different chip types: (a) Si, (b) Si-diamond, (c) diamond and with various heater powers. (d) Normalized temperature distribution for the three different chip types at a flow rate of 5 ml/min and heater power of $q'' = 190$ W/cm^2 to emphasize the enhanced heat distribution with increased diamond layer.

diamond layer and about 34% using only a 400-μm diamond layer. Temperature spatial distribution on the width of a silicon surface of the device at a heat flux of 38 W/cm^2 is studied for different time intervals of heating. The maximum temperature is at the center of the outer surface. After a time interval of 8 s, the differences between the temperatures at the center and at the edge of the outer surface are 5, 3, and 1 °C for cases without a diamond layer, with a 100-μm diamond layer, and with only a 400-μm diamond, respectively.

At steady-state conditions, the experiments and calculations are done assuming a small volumetric flow rate of water through the microchannel cooler (maximum flow rate of 5 ml/min). However, if required by system constraints, the flow can be enhanced considerably, even without changing the design of the channel structure. At a heat flux of 190 W/cm^2 and flow volume rates of 2–5 ml/min, the surface temperature decreases about 15% for a silicon wafer with a 100-μm diamond layer and about 22% for only a 400-μm diamond layer. At a heat flux of 100 W/cm^2 and flow volume rates of 2–5 ml/min, the surface temperature decreases about 11% for a silicon wafer with a 100-μm diamond layer and about 15% for only a 400-μm diamond layer.

We demonstrate that the combination of diamond layers and microfluidics results in enhanced cooling due to combined heat spreading and heat dissipation due to convection. The effect is shown to become significant with increasing operating power. Also, there is good agreement between the experiments and the numerical simulations for both transient and steady-state responses. Future work will focus on examining the potential of using the diamond layer as a cold plate that contacts the active layer via a thin thermal interface material (TIM). We will also examine different fabrication techniques for the production of microchannels within the diamond layer (e.g., direct laser cutting, selective nucleation). Finally, we will examine the integration of PDMS channels directly on top of the active layer by adding a thin insulation layer.

ACKNOWLEDGMENTS

We acknowledge funding by the Center for Security science and Technology (CSST) Grant No. 2024384. The fabrication of the chip was made possible through the financial and technical support of the Technion RBNI (Russell Berrie Nanotechnology Institute) and MNFU (Micro Nano Fabrication Unit.

[1] A. Bar-Cohen, J. J. Maurer, and J. G. Felbinger, in CS MANTECH Conference, May 13th–16th (2013). http://csmantech.pairserver.com/newsite/gaasmantech/Digests/2013/papers/050.pdf

[2] G. Hetsroni, A. Mosyak, E. Pogrebnyak, and L. P. Yarin, Fluid flow in micro-channels, Int. J. Heat Mass Transf. **48**, 1982 (2005).

[3] Y. Mizuno *et al.*, in Electronic Components and Technology Conference (ECTC), 2011 IEEE 61st. IEEE (2011). https://ieeexplore.ieee.org/abstract/document/5898715

[4] M. V. Corbin *et al.*, *Diamond Microchannel Heat Sink Designs for High Heat Flux Thermal Control* (RAYTHEON CO TEWKSBURY MA ELECTRONIC SYSTEMS DIV, 2002). https://apps.dtic.mil/docs/citations/ADA408712

[5] D. L. Blackburn, in Semiconductor Thermal Measurement and Management Symposium, 2004. Twentieth Annual IEEE (IEEE, 2004). https://ieeexplore.ieee.org/abstract/document/1320455

[6] M. Kuball, G. J. Riedel, J. W. Pomeroy, A. Sarua, M. J. Uren, T. Martin, K. P. Hilton, J. O. Maclean, and D. J. Wallis, Time-resolved temperature measurement of AlGaN/GaN electronic devices using micro-raman spectroscopy, IEEE Electron Device Lett. **28**, 86 (2007).

[7] D. C. Knupp, R. M. Cotta, C. P. Naveira-Cotta, and S. Kakaç, Transient conjugated heat transfer in microchannels: Integral transforms with single domain formulation, Int. J. Therm. Sci. **88**, 248 (2015).

[8] Q. Diduck, J. Felbinger, L. F. Eastman, D. Francis, J. Wasserbauer, F. Faili, D. I. Babić, and F. Ejeckam, Frequency performance enhancement of AlGaN / GaN HEMTs on diamond, Electron. Lett. **45**, 758 (2009).

[9] M. Alomari, A. Dussaigne, D. Martin, N. Grandjean, C. Gaquie, and E. Kohn, AlGaN / GaN HEMT on (111) single crystalline diamond, Electron. Lett. **46**, 299 (2010).

[10] A. Rogacs and J. Rhee, in Advanced Packaging Materials: Processes, Properties, and Interfaces, 2007. APM 2007. 12th International Symposium on (IEEE, 2007). https://ieeexplore.ieee.org/abstract/document/4419929

[11] A. Wang, M. J. Tadjer, and F. Calle, Simulation of thermal management in AlGaN/GaN HEMTs with integrated diamond heat spreaders, Semicond. Sci. Technol. **28**, 055010 (2013).

[12] M. Seelmann-eggebert, P. Meisen, F. Schaudel, P. Koidl, and A. Vescan, Heat-spreading diamond films for GaN-based high-power transistor devices, Diam. Relat. Mater. **10**, 744 (2001).

[13] M. Alomari, M. Dipalo, S. Rossi, M.-A. Diforte-Poisson, S. Delage, J.-F. Carlin, N. Grandjean, C. Gaquiere, L. Toth, B. Pecz, and E. Kohn, Diamond overgrown InAlN / GaN HEMT, Diam. Relat. Mater. **20**, 604 (2011).

[14] K. E. Goodson, K. Kurabayashi, and R. F. W. Pease, Improved heat sinking for laser-diode arrays using microchannels in CVD diamond, IEEE Trans. Components Packag. Manuf. Technol. Part B **20**, 104 (1997).

[15] J. P. Calame, R. E. Myers, S. C. Binari, F. N. Wood, and M. Garven, Experimental investigation of microchannel coolers for the high heat flux thermal management of GaN-on-SiC semiconductor devices, Int. J. Heat Mass Transf. **50**, 4767 (2007).

[16] Y. Han *et al.*, in Electron Devices and Solid-State Circuits (EDSSC), 2015 IEEE International Conference on (IEEE, 2015). https://ieeexplore.ieee.org/abstract/document/7285187

[17] See Supplemental Material at http://link.aps.org/supplemental/10.1103/PhysRevApplied.11.014047 for additional figures.

[18] T. L. Bergman, A. S. Lavigne, F. P. Incropera, and D. P. Dewitt, *Fundamentals of Heat and Mass Transfer* (2011) 7th ed., p. 1076.

[19] M. A. Angadi, T. Watanabe, A. Bodapati, X. Xiao, O. Auciello, J. A. Carlisle, J. A. Eastman, P. Keblinski, P. K. Schelling, and S. R. Phillpot, Thermal transport and grain boundary conductance in ultrananocrystalline diamond thin films, J. Appl. Phys. 99, **114301** (2016).

[20] Diamond Materials, The CVD diamond booklet, *Online Cat.*, 4 (2014).

[21] M. Chandran, S. Elfimchev, S. Michaelson, R. Akhvlediani, O. Ternyak, and A. Hoffman, Fabrication of microchannels in polycrystalline diamond using prefabricated Si substrates, J. Appl. Phys. **122**, 145303 (2017).

[22] D. Klein, G. Hetsroni, and A. Mosyak, Heat transfer characteristics of water and APG surfactant solution in a micro-channel heat sink, Int. J. Multiph. Flow **31**, 393 (2005).

[23] Z. Zhang and Y. Li, CFD simulation on inlet configuration of plate-fin heat exchangers, Cryogenics (Guildf). **43**, 673 (2003).

[24] R. W. Barber and D. R. Emerson, Optimal design of microfluidic networks using biologically inspired principles, Microfluid. Nanofluidics **4**, 179 (2008).

[25] A. Parahovnik, N. Tzabar, Y. Haas, L. Parahovnik, I. Rosinsky, and G. Yossifon, Evaluation of axial conduction effects and heat losses in counter-flow microscale heat exchangers, Appl. Therm. Eng. **121**, 1095 (2017).

[26] G. Hetsroni, M. Gurevich, A. Mosyak, and R. Rozenblit, Surface temperature measurement of a heated capillary tube by means of an infrared technique, Meas. Sci. Technol. **14**, 807 (2003).